ELSEVIER

Volume 181, Number 3, March 2008

JOURNAL OF SOLID STATE CHEMISTRY

www.elsevier.com/locate/jssc

CONTENTS

Abstracted/indexed in BioEngineering Abstracts, Chemical Abstracts, Coal Abstracts, Current Contents/Physics, Chemical, & Earth Sciences, Engineering Index, Research Alert, SCISEARCH, Science Abstracts, and Science Citation Index. Also covered in the abstract and citation database SCOPUS®. Full text available on ScienceDirect®.

Regular Articles

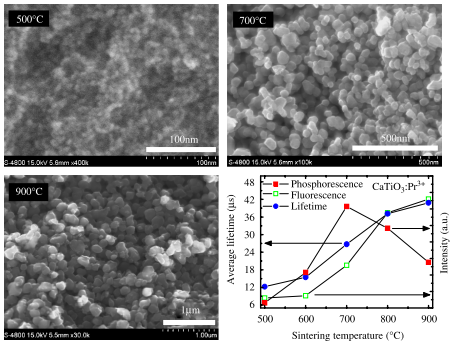

The dependence of fluorescence and phosphorescence on annealing temperature in $CaTiO_3:Pr^{3+}$ nanoparticles prepared by a coprecipitation technique.

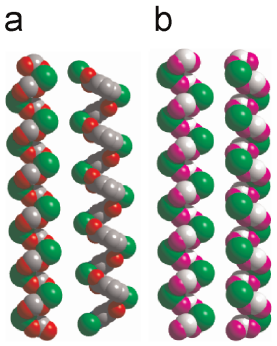

Two copper helical coordination polymers, $[Cu(2\text{-pc})(3\text{-pc})]_n$ **1** and $[Cu(2\text{-pc})(4\text{-pc})]_n$ **2** have been obtained by hydrothermal synthesis. Both two compounds crystallized in non-centrosymmetric space groups, $P2_12_12_1$ and $Pna2_1$, respectively. The 3D framework of **1** is constructed from right-handed helical Cu(2-pc) chains and left-handed Cu(3-pc) helices. As for **2**, Cu(2-pc) helical chains, in which left- and right-handed helices are coexisting, and Cu(4-pc) zigzag chains combined together to form 3D architecture of 2 as well.

Regular Articles—Continued

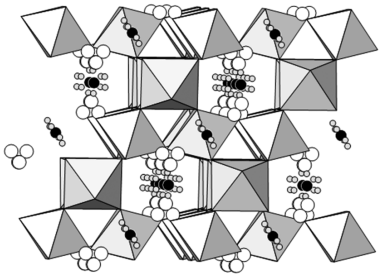

Crystal structures of the pyrochlores $Ca_{1.46}Ti_{1.38}Nb_{1.11}O_7$ and $Ca_{1.51}Ti_{1.32}V_{0.04}Ta_{1.10}O_7$ were refined using single-crystal X-ray diffraction data. Both Ca^{2+} and Ti^{4+} occupy the A-type sites; Ca occupies the ideal 16*d* site and Ti is displaced 0.7 Å to partially occupy a ring of six 96*g* sites. The O′ oxygens are disordered among a tetrahedral cluster of 32*e* sites displaced 0.48 Å from the ideal 8*b* site. Both pyrochlores display dielectric relaxation similar to that observed for analogous Bi-based systems.

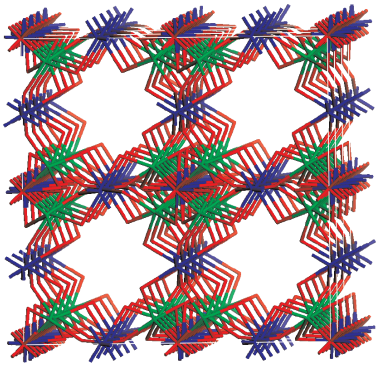

A three-dimensional quaternary chalcogenide $[Na_5Zn_{3.5}Sn_{3.5}S_{13}]\cdot 6H_2O$ represents an interesting example of chalcogenide based semiconductor that combines semiconductivity, porosity, and light emission in a single structure. The electronic and optical properties of this compound can be systematically tuned by substitution of metal and chalcogen elements.

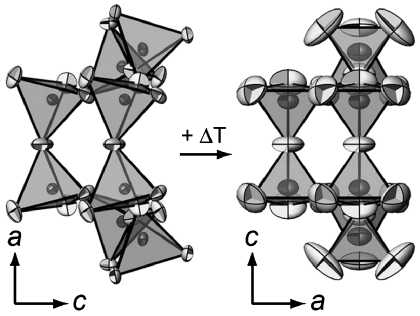

Temperature-dependent structural evolution of microporous $CsAlSi_5O_{12}$ has been investigated by single-crystal and powder X-ray diffraction, as well as Raman spectroscopy. Results yielded a phase transition of order–disorder type.

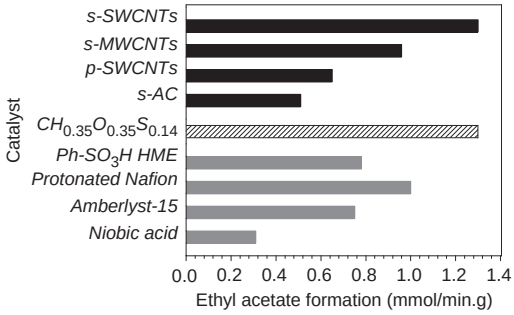

Sulfonated SWCNTs with 20 wt% $-SO_2OH$ groups were prepared by a high-temperature H_2SO_4 process, which transformed the hydrophobic surface of pristine SWCNTs to a hydrophilic surface and provided an excellent performance as solid acid catalyst.

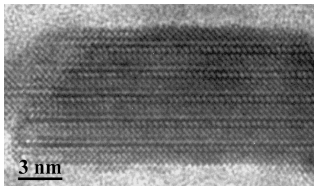

$Bi_{3.25}La_{0.75}Ti_3O_{12}$ nanoplatelets, of which the thickness downs to one cell parameter along the *c*-axis, are obtained through a soft chemical lithiation process followed by exfoliation. Li^+ cations intercalate in the intermediate $(Bi_2O_2)^{2+}$ layers. However, not all of them actually accommodate lithium. Moreover, exfoliation is destructive for the host layers.

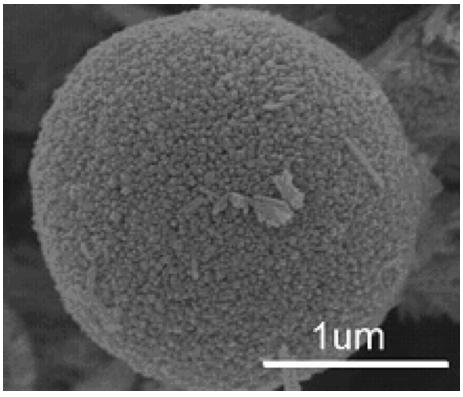

Rutile-phase TiO_2 powders with novel 3D dandelion-like structures were synthesized. This kind of 3D artificial hierarchical titania structure has the advantage of reserving the novel nanometer-scale properties while providing us the easiness of storing and handling as we routinely enjoyed for the micrometer-scale materials. A different oxidation process of Ti(III) to Ti(IV) during hydrothermal process was suggested.

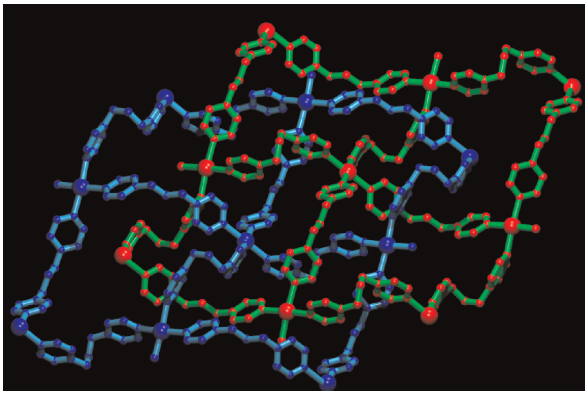

Complexes of $[M_2(bpp)_4X_4]$ [*M*, Fe(II)/Co(II); bpp, 4,4′-trimethylenedipyridine; *X*, SCN^-, $SeCN^-$ and $N3^-$] have been synthesized. The structural analysis reveals undulated 2D network with (4,4) net topology adopting two different conformations of bpp alternately. Two such networks undergo parallel interpenetration. Pseudohalides are observed to help in stacking the interpenetrated nets through hydrogen bonding.

Continued

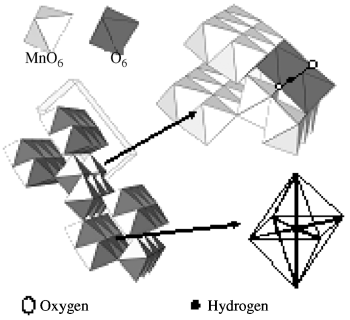

Proposed model for the position of 'Ruetschi' and 'Coleman' proton inside manganese dioxide.

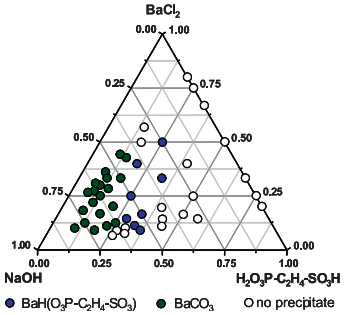

The synthesis of the ligand $H_2O_3P–C_2H_4–SO_3H$ and its use in the systematic investigation in the system $BaCl_2/H_2O_3P–C_2H_4–SO_3H/NaOH/H_2O$ led to the new barium phosphonatosulfonate $BaH(O_3P–C_2H_4–SO_3H)$.

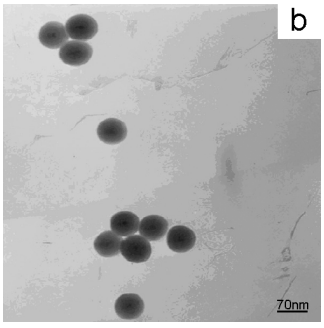

Fig. 2b shows TEM images of silica-coated Fe_3O_4 particles. The magnetic silica particles with well-defined core/shell structures were rather monodisperse, even though silica shells have trapped more than one magnetic core. The Fe_3O_4/SiO_2 particles used in this case for the production of composite particles had an average diameter of 70 ± 10 nm obtained by TEM images.

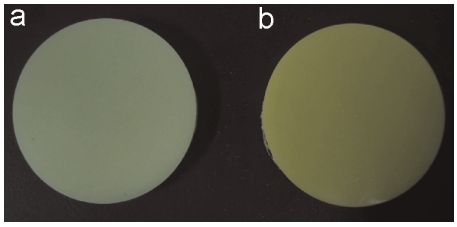

A new class of environmentally benign rare earth pigments of general formula $Pr_{2-x}Ca_xMo_2O_{9-\delta}$ (x ranges from 0 to 1.0) displaying colors ranging from green to yellow were synthesized by traditional solid-state route, as alternatives to lead, cadmium and chromium colorants. The yellow–green pigments were found to be interesting alternatives to existing toxic pigments for coloration of plastics.

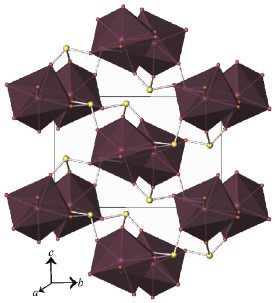

A depiction of the three-dimensional structure of $Pu(SeO_3)_2$ formed from the interconnection of one-dimensional chains of edge-sharing PuO_8 dodecahedra by selenite anions.

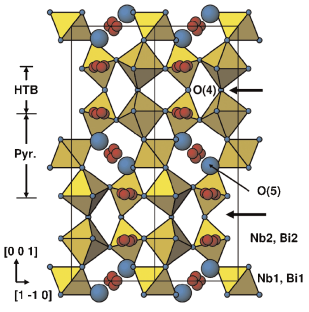

[110] polyhedral projection of the structure of $Bi_{3.32}Nb_{7.09}O_{22.7}$. Heavy arrows show location of chemical twin planes.

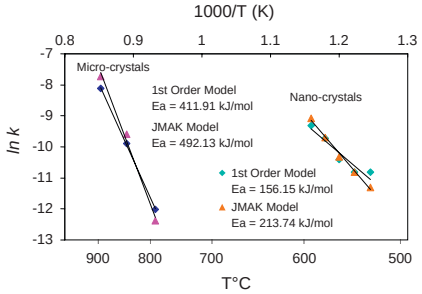

The transformation kinetics from titania brookite to rutile can be described by both the standard first-order model and the JMAK model. The obtained activation energy for micron-sized brookite crystals is much higher than that for brookite nano-crystals.

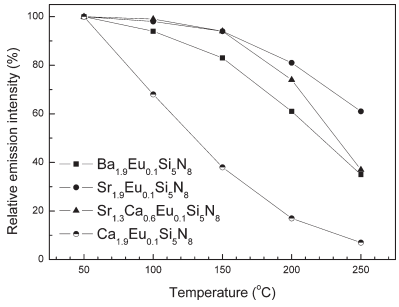

The temperature dependence of the luminescence efficiency of $M_{1.9}Eu_{0.1}Si_5N_8$ (M = Ca, Sr, Ba) and $Sr_{1.3}Ca_{0.6}Eu_{0.1}Si_5N_8$ (λ_{exc} = 465 nm).

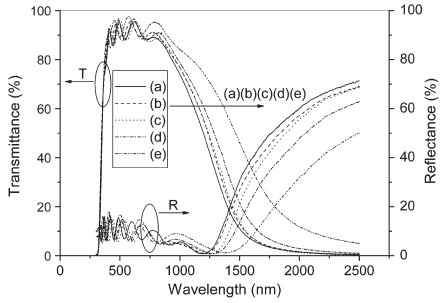

The figure shows transmittance and reflectance spectra of $Zn_{1-x}Mg_xO$:Ga films measured in the wavelength range of 300–2500 nm. In the visible region the films are highly transparent, and their spectra are like those of dielectrics regardless of Mg content. In the IR region the films behave like metals and have high reflectance and low transmittance.

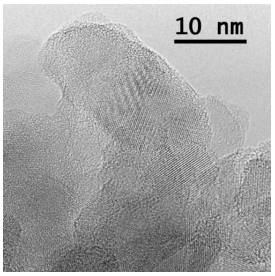

Ammonolysis reactions of Me_3N–$Al(NHDipp)_3$ in liquid NH_3 yielded Al–N oligomers, which can be transformed into nanocrystalline aluminum nitride particles under thermolysis conditions at 1000 °C. Theoretical calculations were performed in order to identify potential reaction intermediates.

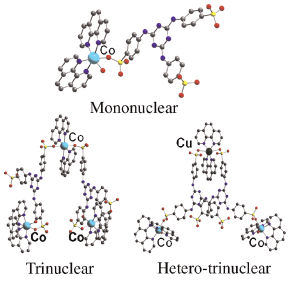

Novel mononuclear, trinuclear, and hetero-trinuclear supermolecular complexes, $[Co(phen)_2(H_2O)(HTST)]\cdot 2H_2O$ (**1**), $[Co_3(phen)_6(H_2O)_2(TST)_2]\cdot 7H_2O$ (**2**), and $[Co_2Cu(phen)_6(H_2O)_2(TST)_2]\cdot 10H_2O$ (**3**), have been synthesized by the reactions of a new tri-sulfonate ligand (2,4,6-tris(4-sulfophenylamino)-1,3,5-triazine, H_3TST) with the M^{2+} (M = Co, Cu) and the second ligand 1,10-phenanthroline (phen). The study shows the flexible multifunctional self-assembly capability of H_3TST ligand presenting in these supramolecular complexes.

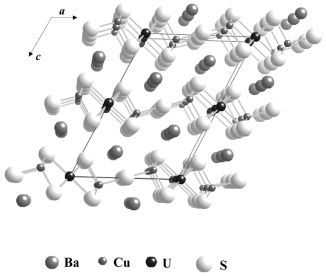

Unit cell of $Ba_2Cu_2US_5$ viewed down [010].

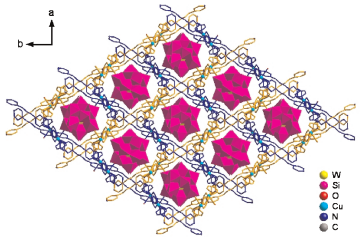

Compound $[Cu_2(bpp)_4(H_2O)_2](SiW_{12}O_{40})\sim 6H_2O$ (**1**) represents the first 2-D interpenetrating cationic metal–organic frameworks (MOFs) templated by Keggin-type anions. These MOF layers are stacked together along the crystallographic *c* axis exactly to construct large cubic-like channels (with dimensions of 12.3 × 13.6 Å) occupied by $SiW_{12}O_{40}^{4-}$ clusters.

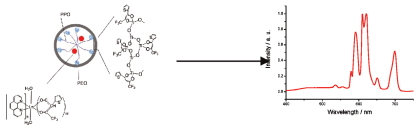

Novel stable luminescent organic–inorganic hybrid titania thin film with high transparency activated by *in-situ* formed lanthanide complexes have been obtained at room temperature via a simple one-pot synthesis approach by using TTFA-modified titanium precursor with amphiphilic triblock copolymer P123. The obtained hybrid thin film displays bright red (or green), near-monochromatic luminescence due to the *in-situ* formed lanthanide complex.

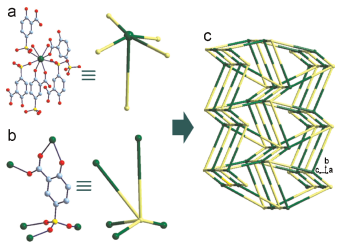

Syntheses and crystal structures of four 3D lanthanide-5-sulfosalicylates, $Ln(SSA)(H_2O)_2$ [Ln = Ce(III) (**1**), Pr(III) (**2**), Nd(III) (**3**), and Dy(III) (**4**)], have been reported. In complexes **1–4**, Ln(III) acting as 5-connected inorganic node and SSA^{3-} ligand acing as 5-connected organic node interlink into rarely reported $4^6 6^4$ topology network. Luminescence and magnetism properties have also been studied.

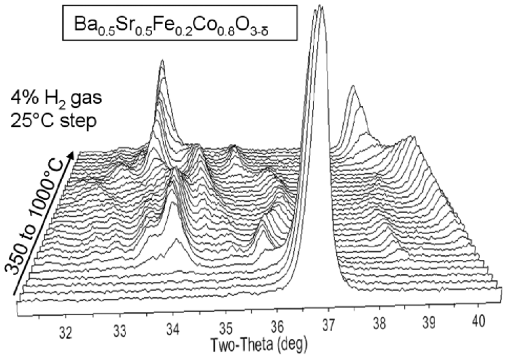

The phase stability of the fuel cell cathode $Ba_{0.5}Sr_{0.5}Fe_{1-x}Co_xO_{3-\delta}$ in low pO_2 and high temperature has been investigated using *in situ* X-ray diffraction. Both stability and thermal expansion coefficient were found to increase with increasing iron content. Decomposition products under reducing conditions have been identified.

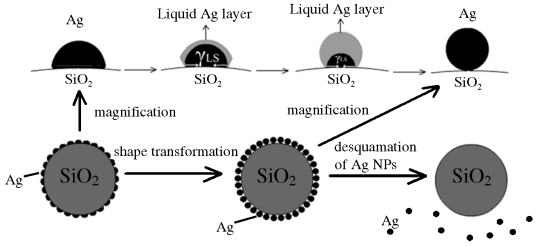

The shape evolution and thermal stability of Ag nanoparticles (NPs) on spherical SiO_2 substrates were investigated by means of *in situ* TEM imaging and DSC analysis. A possible mechanism for the desquamation of Ag NPs from the SiO_2 sphere surface is proposed. Here, a simple sketch is shown to describe the shape evolution and desquamation process of the Ag NPs.

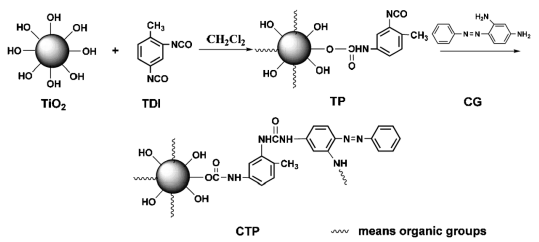

Dye-modified TiO_2 photocatalysts were synthesized via the reaction between Chrysoidine G (CG), Degussa P25 (TiO_2), and tolylene-2,4-diisocyanate (TDI) as a bridging molecule. As a result, π-conjugated surface organic complexes were formed on TiO_2 surface. Due to the existence of organic complexes, dye-modified TiO_2 catalysts showed great visible absorption and high activity under the visible light irradiation.

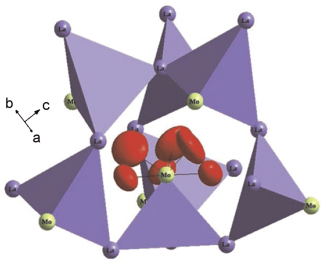

Anti-tetrahedral unit centred in O1 and linked through La ions to form a cage where the partially occupied O2 and O3 ions are placed.

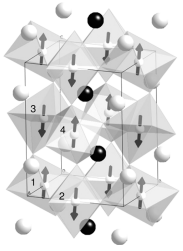

A neutron diffraction study shows that the perovskite $BiNiO_3$ retains the unusual charge distribution $Bi^{3+}_{0.5}Bi^{5+}_{0.5}Ni^{2+}O_3$ down to 5 K. The Ni^{2+} moments are ordered in the *G*-type antiferromagnetic arrangement shown; however, $BiNiO_3$ is ferrimagnetic due to the inexact cancellation of the four inequivalent moments in the triclinic unit cell.

At the end of the 20th century, a new concept of battery was introduced, named "Li ion", where electrodes are both lithium-storage materials. Compounds with a spinel structure are so investigated and microwave heating appears as an efficient source of energy to produce nanoparticles in a very short time and at low temperature, with controlled size (4–5 nm) and high specific area ($240\ m^2/g$).
Legend: Pictogram represents our original microwave reactor, the RAMO (French acronym of Réacteur Autoclave Micro-Onde), containing the reactants and submitted to the microwave irradiation. Multicolor candy represents obtained material.

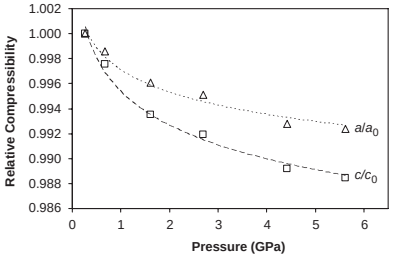

Relative compressibility of the lattice parameters of a new osmate, Sr_2CuOsO_6.

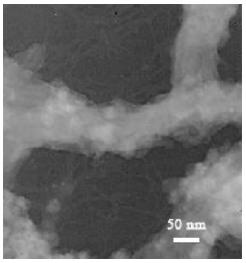

The work on preparing nanocomposites has been too much, but few reports were about synthesizing one-dimensional nanocomposite of three different nanoscale materials. In our work, we prepared one-dimensional multiwalled carbon nanotubes/Fe_3O_4 particles/polyaniline composite nanotubes and studied their conductive and magnetic properties.

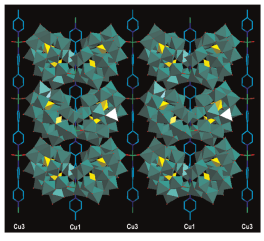

Two Dawson-based phosphotungstates $(H_2en)_{0.5}H[Cu(en)_2(H_2O)]_2\{[Cu(en)_2](\alpha_1\text{-}P_2W_{17}CuO_{61})\}\cdot 8H_2O$ (**1**) and $[4,4'\text{-}H_2bpy]_2\{[Cu(4,4'\text{-}bpy)_3][Cu(4,4'\text{-}bpy)_4(H_2O)_2]_2[Cu(4,4'\text{-}bpy)][\alpha\text{-}P_2W_{18}O_{62}]_2\}\cdot 6H_2O$ (**2**) have been hydrothermally synthesized and structurally characterized. **1** consists of a 1-D linear chain structure constructed from monocopper-substituted Dawson polyoxoanions, while **2** represents the first 2-D sheet-like structure with a (4,4)-connected topological net built up from saturated Dawson-type polyoxoanions and Cu^{II}-4,4′-bpy complex cations in polyoxometalate chemistry.

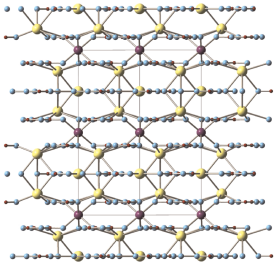

A new compound $Ba_3InB_9O_{18}$ was synthesized with space group $P6_3/m$, lattice parameters $a=7.1359(3)$ Å, $c=16.6151(8)$ Å, $Z=2$ and $V=723.697$ Å^3. Its crystal structure is made up of planar B_3O_6 groups, regular InO_6 octahedra, irregular BaO_6 hexagons and BaO_9 polyhedra. Its XEL spectra show an intense emission band in the range of 360–500 nm with light yield about 75% of BGO.
The projection of the $Ba_3InB_9O_{18}$ structure along the 〈11–20〉 direction.

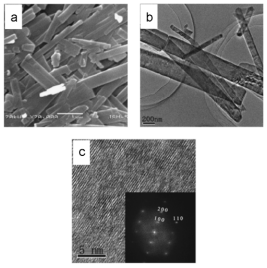

Selective-controlled structure and shape of ammonium vanadate nanocrystals were successfully synthesized by a simple hydrothermal method without the presence of catalysts or templates. The final products were $NH_4V_4O_{10}$ nanobelts, $(NH_4)_2V_6O_{16}\cdot 1.5H_2O$ nanowires, and $(NH_4)_6V_{10}O_{28}\cdot 6H_2O$ nanobundles, respectively, when the pH of the growth solution varied from 2.5 to 1.5, then to 0.5.

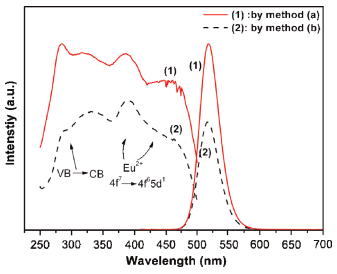

The Eu^{2+}- and Ce^{3+}-doped $CaAl_2S_4$ phosphors were comparatively synthesized by two methods. The emission intensity of Eu^{2+} ion in sample synthesized by the evacuated sealed quartz ampoule method is by a factor of 1.7 as strong as that of Eu^{2+} ion in sample prepared by the conventional solid-state reaction method.

Rapid Communications

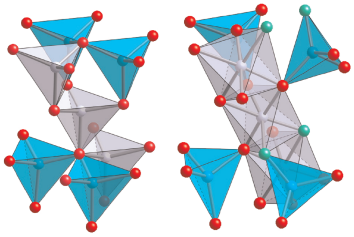

A new mixed-metal oxide of composition $YBaCo_4O_{8.1}$ has been synthesized by controlled oxidation of $YBaCo_4O_7$ and its structure determined using neutron and synchrotron X-ray powder diffraction. The structure features two alternating layers: a triangular layer of isolated CoO_6 octahedra and CoO_4 tetrahedra that links distorted Kagomé planes of charge-ordered Co ions. In these planes, a rarely observed motif of zigzag rows of edge-sharing octahedra is found, which are connected by ribbons of corner-sharing tetrahedra.

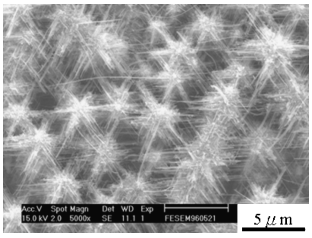

The novel three-dimensional hierarchical structure is composed of single-crystalline Zn microtips with the converted ZnO coating as stem, and ZnO nanowhiskers as branches. The branched ZnO nanowhiskers exhibit preferred growth direction, suggesting that the branched nanostructures might have a preferred orientation, and maintain a well-defined relationship to the Zn stem.

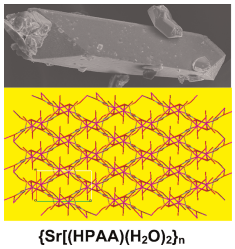

$\{Sr[(HPAA)(H_2O)_2]\}_n$

Syntheses, characterization and crystal structures of metal-hydroxyphosphonoacetate hybrids are reported (Metal = Sr, Ba). 2D and 3D materials were prepared. Their anti-corrosion effects were studied at pH 2.0 and 7.3. It was found that anti-corrosion efficiency was demonstrated only at pH 7.3.

Continued

Author inquiries

Submissions

For detailed instructions on the preparation of electronic artwork, consult the journal home page at http://authors.elsevier.com.

Other inquiries

Visit the journal home page (http://authors.elsevier.com) for the facility to track accepted articles and set up e-mail alerts to inform you of when an article's status has changed. The journal home page also provides detailed artwork guidelines, copyright information, frequently asked questions and more.

Contact details for questions arising after acceptance of an article, especially those relating to proofs, are provided after registration of an article for publication.

Language Polishing

Authors who require information about language editing and copyediting services pre- and post-submission should visit http://www.elsevier.com/wps/find/authorshome.authors/languagepolishing or contact authorsupport@elsevier.com for more information. Please note Elsevier neither endorses nor takes responsibility for any products, goods, or services offered by outside vendors through our services or in any advertising. For more information please refer to our Terms & Conditions at http://www.elsevier.com/wps/find/termsconditions.cws_home/termsconditions.

For a full and complete Guide for Authors, please refer to *J. Solid State Chem.,* Vol. 180, Issue 1, pp. *bmi–bmv*. The instructions can also be found at http://www.elsevier.com/wps/find/journaldescription.cws_home/622898/authorinstructions.

Journal of Solid State Chemistry has no page charges.